Scaling properties of centering forces

Serge Dmitrieff, Nicolas Minc

Scaling properties of centering forces.

Serge Dmitrieff* and Nicolas Minc
Institut Jacques Monod CNRS UMR7592 and Universite Paris Diderot
75205 Paris Cedex 13 France

Motivated by the centering of microtubule asters in cells, we study the general properties of three types of centering forces : bulk pulling forces, surface (cortical) pulling forces, and pushing forces. We evidence unexpected scaling laws between the net force on the aster and its position for different modes of centering, and also address how the effective centering stiffness depends on cell size. Importantly, we find that both scaling laws and effective stiffness depend on the spatial dimensions, and thus that 1D and 2D ansatz usually considered could misguide the interpretation of experimental results. We also show how scaling laws depend on cell shape. While some hold for any convex cell, others strongly depend on the shape. By deriving these scaling laws for any spatial dimension, we generalize these results beyond the biological perspective. This analysis provides a broad framework to understand shape sensing mechanisms.

In animal eggs after fertilization, the male pronucleus reaches the center of the cell, seemingly following only geometrical cues : in deformed cells, the pronucleus seems to stop at the center of mass [1]. It is remarkable that a small biological object can robustly find the center of the containing space autonomously. It has thus gained a lot of experimental and theoretical attention. The pronucleus creates an aster, a radial structure of stiff elastic filaments called microtubules. Molecular motors attached to structures in the cell volume (such as vesicles or the endoplasmic reticulum) and/or to the surface (the cell cortex) pull on microtubules, while microtubule growth creates a pushing force when they are in contact with the cell cortex. In many species, a combination of these mechanisms allows for efficient aster centration [2–6]. However, which of bulk pulling, cortical pulling, or pushing is dominating in a given species, remains controversial [7].

While more biochemical and biophysical methods become available to address this issue, surprisingly little is known on how the cell-scale centering forces depend on how forces are applied on individual microtubules. In this article, we aim at clarifying the mathematical properties of centering forces according to the centering mechanism. We use a single formalism to encompass three different mechanisms, and study their scaling properties, i.e. how the integrated force on the aster scales with the aster distance to the cell center, and how the effective centering stiffness scales with cell size. We find that some centering mechanisms exhibit surprising scaling properties. We first focus on biologically relevant case studies before generalizing to an agent seeking the center of a space in n dimensions. This allows us to address how centering forces depend on dimensionality and container geometry.

* serge.dmitrieff@ijm.fr

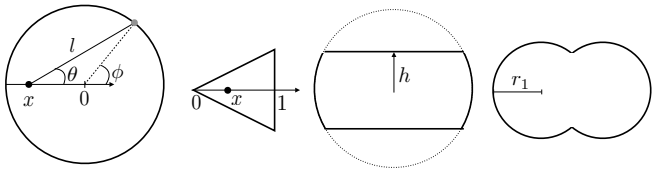

FIG. 1. Illustration of the shapes considered, in the Oxy plane. From left to right : sphere, cone, truncated ball, doublet. In 3D, all shapes are symmetric around their Ox axis.

I. CENTERING BY BULK PULLING

We consider an aster centering by motors in the cell volume pulling on microtubules emanating from the aster. Let us call R the radius of the cell if it is spherical, or its characteristic size otherwise and l the length of a microtubule normalized by R ; the pulling force on the microtubule should depend on the number of motors attached to it, and thus upon l. It is generally assumed that the magnitude of the force on a microtubule is $f_1 l^p$, where p is an exponent describing the interaction of the microtubule with motors, and f_1 is a typical force. For instance, we expect a scaling exponent $p = 1$, if motors are not limiting, so that they saturate the microtubule length, and $p = 3$ if motor attachment is limited by the availability or binding time of motors [1, 8, 9]. The microtubule length l should depend upon its orientation θ and upon x the position of the aster normalized by R. Calling N the total number of microtubules, the net force on the aster projected on the axis Ox reads :

$$\bar{f}^p(x) = \frac{N f_1}{2} \int_0^\pi l(x,\theta)^p \cos\theta \sin\theta \, d\theta \,. \qquad (1)$$

Here we averaged over all filament orientations θ (see Fig. 1, left), and implicitly integrated over all orientations around the Ox axis (as is described by the factor $\sin\theta$), assuming microtubules to have a uniform angular distribution. Because we are interested in scaling properties rather than dynamics, we will not consider the early stages when the aster is small, and always assume that

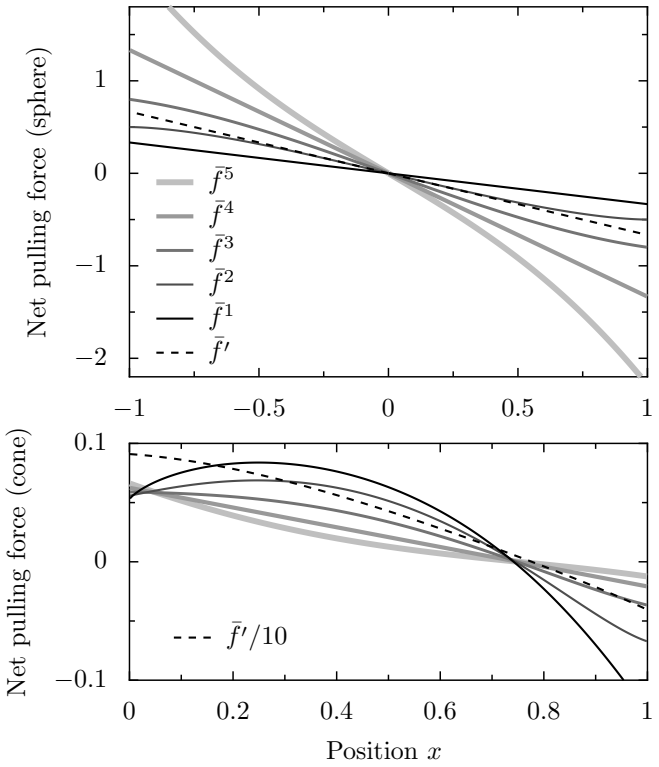

FIG. 2. *Top* : Net centering force in a spherical cell by bulk pulling forces of different power law $\bar{f}^p$ and by cortical pulling $\bar{f}'$, as a function of the position x (where x is normalized by the typical size R). *Bottom* : centering forces by bulk and cortical pulling in a conical cell (here the cortical pulling force was scaled for visual convenience). Bulk and cortical pulling forces are normalized by Nf_1 and Mf_m respectively (see text).

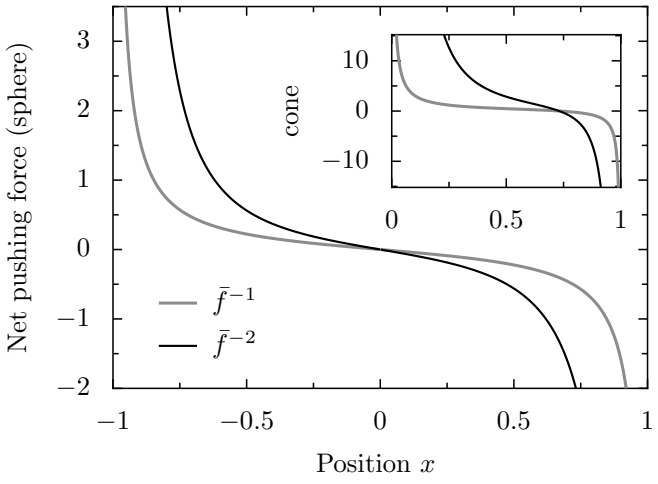

FIG. 3. *Top* : Net centering force in a spherical cell by bulk pulling forces of different power law $\bar{f}^p$, as a function of the position x (where x is normalized by the typical size R). $p = -1$ corresponds to dynamic microtubules and $p = -2$ to buckling microtubules. *Insert* : centering forces by pushing in a conical cell. Forces are normalized by Nf_1 (see text).

microtubules have grown long enough so that they are all touching the cortex. In this case the function $l(x, \theta)$ depends on the shape of the cell. In a sphere, we have :

$$l(x, \theta) = -x \cos\theta + \sqrt{1 - x^2 \sin^2\theta}\,, \tag{2}$$

Taking the specific case of a spherical cell, we already see interesting scaling properties, Fig. 2. For $p = 1$, $\bar{f}^1(x)$ is linear with x as could be expected. Remarkably, we find that $\bar{f}^4$ is also linear with x, but that $\bar{f}^2$ and $\bar{f}^3$ are sub-linear, although the forces per microtubule length are super-linear with microtubule length. Only for $p > 4$ (e.g. $p = 5$) does the net force $\bar{f}^p$ becomes super-linear with x, see Fig. 2. We will see later that these power laws depend on the dimension considered. To understand if these results hold in non-spherical geometries, we considered a conical cell shape (see Fig. 1) -mimicking that of cells confined in microfabricated chambers [1] - and found that $\bar{f}^1$ is no longer linear with x ; $\bar{f}^1$, $\bar{f}^2$ and $\bar{f}^3$ are now non-monotonous with x and $\bar{f}^5$ is still super-linear (Fig. 2). Interestingly, $\bar{f}^4$ is still linear with x. We will see in the second part of this article that this corresponds to a more general result: in an $n-$dimensional convex space, the centering force for $p = n + 1$ is always linear. Centering in cells is often described by a stiffness, i.e. the stiffness of an elastic potential that would yield the same force profile [2, 10]. Although we can only rigorously identify a centering stiffness when the force is linear with x (e.g. for $\bar{f}^4$), we can define an *effective* centering stiffness $K = -\partial_x f^p(x = 0)$. For a sphere, we find $K = Npf_1/3R$; for other shapes, we expect the same result up to a geometrical factor γ that depends on p and on cell shape but is independent of R, since all distances can be normalized by R. For bulk pulling forces, the characteristic force f_1 also depends on system size as $f_1 = R^p k_p$. For instance if $p = 1$, k_1 is the motor force per unit microtubule length ; for $p = 3$, k_3 is the force per unit volume, and so on. Therefore, we expect the effective stiffness to be :

$$K = \gamma N p k_p R^{p-1}/3\,, \tag{3}$$

in which $\gamma = 1$ when the cell is spherical. Thus, the dependence of the stiffness on cell size varies with the scaling exponent p. For instance, if the force per microtubule is proportional to their length ($p = 1$), then K is independent of cell size. In addition, we will see later that stiffness also depends on the dimension, and as such, a stiffness estimated in 2D is 50% bigger than that in 3D, i.e. in 3D, one needs 50% more microtubules than would be estimated from a 2D ansatz.

II. CENTERING BY PUSHING

Assuming microtubules to be radially distributed as in bulk pulling, pushing can only work if the force per microtubule depends on its length ; otherwise, we would get a net force $\bar{f}^0(x) = 0$ (see Eqn. 1). Two factors can

contribute to this : microtubule buckling, because the buckling force for a rod depends on its length, and microtubule dynamics, because the time spent pushing on the cortex depends on the distance to the cortex [11]. In the appendix, we show that in the latter case, the fraction of microtubules pushing against the cortex should be l_0/l, with l the normalized distance to the cortex and l_0 a dimensionless parameter comparing the growth speed normalized by R to the catastrophe rate of microtubules at the cortex.

Centering by pushing can therefore be treated similarly to bulk pulling. For dynamic microtubules, we have $p = -1$ and $f_1 = -f_g l_0$, with f_g the polymerization force of a microtubule. f_g should be of a few piconewtons, and independent of microtubule length. For a buckling microtubule, we have $p = -2$ and $f_1 = -f_b$, with f_b the Euler buckling force : $f_b = \pi^2\kappa/R^2$ (with κ the bending modulus of a microtubule [12]). Centering by pushing forces is not linear, and leads to very high forces far from the center, and low forces close to the cell center, see Fig. 3. We can see that the behaviour of these forces depends little on the cell geometry, be it spherical or conical, Fig. 3.

We can use our previous result for the effective stiffness, and we find $K = \gamma N f_g/3R$ for dynamic microtubules and $K = 2\gamma N\kappa\pi^2/3R^3$ for buckling microtubules (with $\gamma = 1$ for a spherical cell). We see, that the dependence of the effective stiffness on cell size markedly differs between the two pushing mechanisms, and could thus be used to discern mechanisms at play. Note that assuming a polymerization force of $6pN$ and a microtubule stiffness $\kappa = 2 \times 10^{-23} Nm$ [12], buckling should occur as soon as microtubules are longer than $5\mu m$; we should thus expect that the scaling exponent $p = -2$ shall apply for large cells, and/or when the aster is far enough from the cortex. A spherical cell of size $R \sim 15\mu m$ is thus expected to have a centering stiffness $K = N \times 0.039 pN/\mu m$. The centering stiffness measured in the C. Elegans embryo, which has this typical radius, is $16.4 pN/\mu m$, yielding an estimate of 420 microtubules contributing to centering stiffness [10]. In larger ($R \sim 45\mu m$) sea urchin Embryos, a stiffness $K \sim 60 pN/\mu m$ was measured, leading to nanoNewton-order forces [2]. About 16000 microtubules would be necessary to create a such stiffness by pushing. Indeed, bulk pulling was shown to dominate in this system [2].

A. Centering by cortical pulling

If motors are located on the cell cortex rather than in the bulk, this should result in a net force $\bar{f}(x) = 0$ (see Eqn. 1). Cortical pulling however has been proposed to lead to efficient centering if the number of motors on the cortex is limiting [3], or if microtubule tips can slide on the cortex [13]. In both cases, we cannot write the net force in the same form as Eqn. 1. Here we will consider the case where the number of motors on the cortex is limiting, as this was recently shown to control aster positioning in-vivo [14, 15]. Let us call $\bar{f}'$ the *directed* centering force projected on Ox. With M the number of motors, f_m the force exerted by a single motor, and assuming motors to be uniformely distributed on the surface, we can write :

$$\bar{f}'(x) = \frac{-M f_m}{S} \int_S \mathbf{u}_x \cdot \mathbf{u}_\theta(\mathbf{r}) d^2\mathbf{r}\,, \tag{4}$$

in which S is the cell surface, $d^2\mathbf{r}$ is the surface element and $\mathbf{u}_x \cdot \mathbf{u}_\theta(\mathbf{r}) = \cos\theta$ is the projection of the direction $\mathbf{u}_\theta$ of the microtubule on the x axis. In a sphere, this simplifies to (see Eq. 8) :

$$\bar{f}'(x) = -\frac{2M f_m}{3} x \tag{5}$$

However, this linear scaling seen in a spherical cell is not shape independent and does not hold in a conical cell (see Fig. 2). The centering stiffness thus reads $K = 2\gamma M f_m/3R$ (with $\gamma = 1$ for a spherical cell), and decreases with increasing system size. Were the forces due to cortical pulling, we would thus expect $M \sim 180$ motors to participate in C. Elegans (assuming $f_m \sim 2pN$), while about $12\times$ this number would be required to explain the stiffness measured in sea urchin embryos. Note that, in 2 dimensions, we find $K = M f_m/2R$, therefore the stiffness of a 2D ansatz is 3/4 that of the real 3D system (see hereafter, for the derivation in n dimensions).

B. Generalization to n-dimensional cells

To reach a more general understanding, we now consider centering forces of an agent in any dimension. We will consider the cell as an $n-$ dimensional space that is symmetric around the axis Ox. We will introduce the generalized formalism for bulk pulling (and pushing) and cortical pulling, before discussing the results. In bulk pulling and pushing, forces are averaged on all angular directions from the agent's perspective, and thus we term this mechanism *autonomous* centering. For cortical pulling, the pulling forces are averaged over all the surface points, and thus the agent's motion is controlled by the surface properties [14, 15]. Thus we name this mechanism *directed* centering. We will see that these two mechanisms belong to different universality classes. From now on, all distances will be normalized by R, and forces by $N f_1$ (for *autonomous* centering) or $M f_m$ (for *directed* centering). The generalization of spherical and conical cells embedded in a n-dimensional space are called n-ball and n-cone respectively.

In the case of *autonomous* centering, the net force $\bar{f}_n^p$ (normalized by $N f_1$) is, with Γ the gamma function :

$$\bar{f}_n^p(x) = \frac{1}{\alpha_n} \int_0^\pi \cos\theta \sin^{n-2}(\theta) l(x,\theta)^p d\theta\,. \tag{6}$$

$$\alpha_n = \frac{\Gamma[\frac{n-1}{2}]}{\Gamma[\frac{n}{2}]}\sqrt{\pi}\,, \tag{7}$$

In the general case of *directed* centering, the pulling force could depend on the distance to the surface. The net force $\bar{f'}^p_n(x)$ (normalized by Mf_m) can be written :

$$\bar{f'}^p_n(x) = \frac{1}{S_n}\int_{S_n} \mathbf{u}_x \cdot \mathbf{u}_\theta(\mathbf{r}) l'(x,\mathbf{r})^p d^{n-1}\mathbf{r}\,, \qquad (8)$$

in which S_n is the surface in n dimension, i.e. an $n-1$-dimensional manifold embedded in an n dimensional space. We can see this centering mechanism as a generalization of Newton's shell [16] for forces of different exponents, and for any dimension. In the particular case of a spherical cell we find :

$$\bar{f'}^p_n(x) = \frac{1}{\alpha_n}\int_0^\pi \left(\frac{\cos\phi - x}{l'(x,\phi)}\right)\sin^{n-2}(\phi) l'(x,\phi)^p d\phi\,, \quad (9)$$

$$l'(x,\phi) = \sqrt{1+x^2-2x\cos\phi}\,. \quad (10)$$

It is possible to solve $\bar{f'}^p_n(x)$ analytically, to find, with ${}_2F_1$ the $(2,1)$ hypergeometric function :

$$\bar{f'}^p_n(x) = -Nf_1(1-x)^{p-1} \times({}_2F_1\left(\frac{n+1}{2},\frac{1-p}{2};n;-\frac{4x}{(x-1)^2}\right) +(x-1){}_2F_1\left(\frac{n-1}{2},\frac{1-p}{2};n-1;-\frac{4x}{(x-1)^2}\right)) \quad (11)$$

Note that here we find $\bar{f'}^{-2}_3(x) = 0$ in agreement with Newton's first theorem [16] ; this result is known to be valid only for a sphere in 3 dimensions.

C. Scaling properties and shape dependence

For autonomous centering, we did not find any generic analytical solution for any n, p or any general shape. However, we did find one peculiar scaling for some values of p. For this, we first define the mean distance^p $\bar{l}^p_n$ to the surface :

$$\bar{l}^p_n(x) = \frac{1}{\alpha_n}\int_0^\pi \sin^{n-2}(\theta) l(x,\theta)^p d\theta\,. \qquad (12)$$

Note that $l^n_n(x)$ is the fraction of space visible from x, and is equal to 1 for any convex space. Moreover, for a such convex space,

$$\partial_x l(x,\theta) = -\cos\theta - \frac{\partial_\theta l(x,\theta)}{l(x,\theta)}\sin\theta \qquad (13)$$

And we find that, for any convex shape :

$$\frac{\partial_x \bar{f}^p_n}{p} = \frac{\alpha_{n+2}}{\alpha_n}\left(\frac{p-n-1}{p-1}\right)\bar{l}^{p-1}_{n+2} - \left(\frac{p-n}{p-1}\right)\bar{l}^{p-1}_n \quad (14)$$

Using $\bar{l}^n_n = 1$, we find :

$$\bar{f}^{n+1}_n(x) = -\frac{n+1}{n}x\,. \qquad (15)$$

Therefore, in n dimensions, the net $(n+1)$-force $\bar{f}^{n+1}_n(x)$ is linear with x, explaining the surprising scaling properties we observed in three dimensions. We could not find any general scaling law for $\bar{f}^1_n(x)$, in agreement with our finding in 3D that the shape of $\bar{f}^1_3(x)$ depends on cell geometry, Fig. 2.

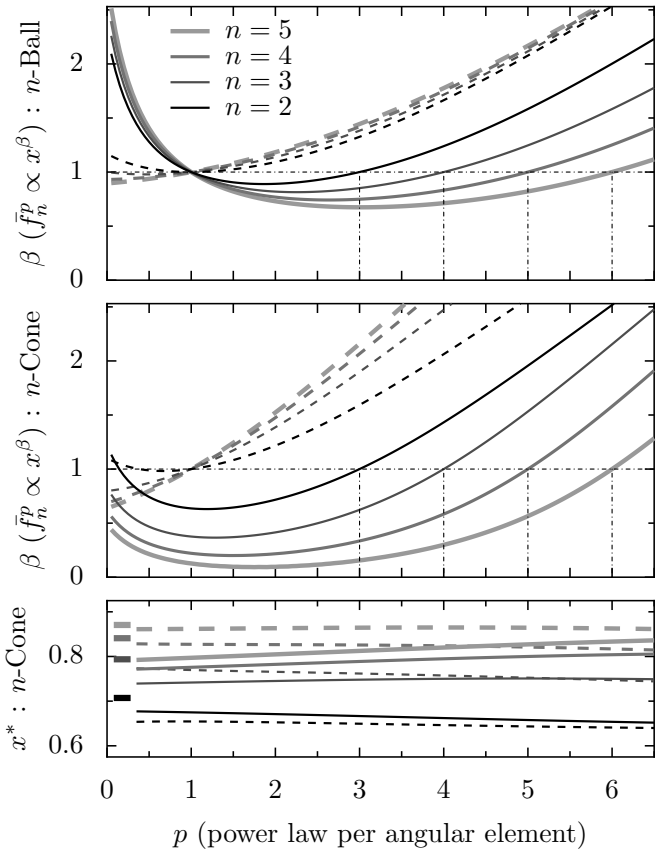

FIG. 4. *Top* : power law β, fitting $\bar{f}^p_n(x) \propto x^\beta$ (autonomous centering, solid lines) and $\bar{f'}^p_n(x) \propto x^\beta$ (directed centering, dashed lines) in a n-ball for different n. *Middle* : same as above, for centering in a n-cone. *Bottom* : equilibrium position x^* such that $\bar{f}^p_n(x^*) = 0$ (solid lines) and such that $\bar{f'}^p_n(x^*) = 0$ (dashed lines) for several n. Thick markers on the left indicate the center of mass of the volume.

To identify universal scaling laws, we systematically computed the power law of $\bar{f}^p_n(x)$ with x. For this, we numerically integrated equations 6, 8, and fitted $\bar{f}^p_n(x)$ by a power law x^β. We could do this in any shape by redefining $l(x,\theta)$ in equation 2. This analysis showed that in a sphere, the net pulling force $\bar{f}^p_n(x)$ is linear with x for $p = 1$ and $p = n+1$, sub-linear in between, and super-linear for $p < 1$ and $p > n+1$, Fig. 4, top. In a cone, the scaling law $\bar{f}^{n+1}_n(x) \propto x$ was still valid but $\bar{f}^1_n(x)$ was no longer proportional to x, as expected. By taking n=3, in the above results, one falls back on the results discussed in the first part of this manuscript for the case of 3D shapes.

Because the scaling behaviour of $\bar{f}^p_n$ depends on the dimension n, it is interesting to consider what happens when one dimension becomes arbitrarily small. For this, we thus integrated Eqs. 12,6 in a 3-ball symmetrically truncated along its Oy axis at a height h, see Fig. 1. We

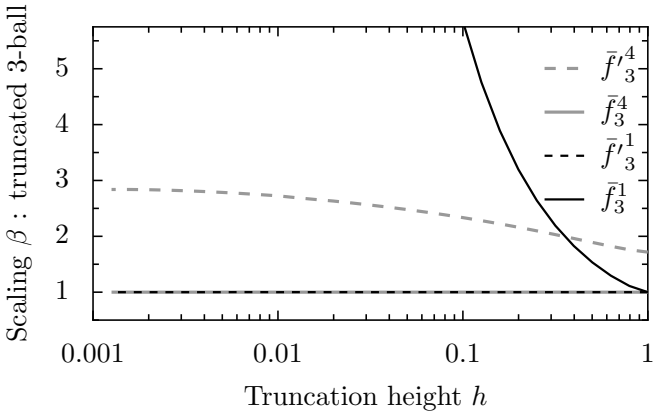

FIG. 5. Fitted power law β for $\bar{f}^p_3(x)$ and $\bar{f}'^p_3(x)$ in a truncated 3-ball (see Fig. 1) as a function of the truncation height h.

found that the expected scaling law for $\bar{f}^4_3$ still held even for $h \to 0$, Fig. 5. Although this was expected from $\bar{l}^n_n$ being space invariant in any convex space, it is interesting to see that a (n)-dimensional system does not behave as $(n-1)$-dimensional system when one dimension becomes infinitesimally small.

For *directed* centering mechanisms, we first consider the simple case $p = 1$, and note that a convex shape symmetric around the axis Ox can be entirely described by a function $r(\phi)$, in which r is the distance from a point on the surface, at angle ϕ to the center of the space. We can thus write :

$$\bar{f}'^1_n \propto \int_0^\pi \left(-x + r(\phi)\cos(\phi)\right)\left(r(\phi)\sin(\phi)\right)^{n-2} d\phi \quad (16)$$

From there, it is clear that $\partial_x \bar{f}'^1_n$ is a constant depending on $r(\phi)$ but not on x. Therefore $\bar{f}'^1_n$ is always linear with x in a convex space. However, we could not find such argument for $\bar{f}'^0_n$; this is in agreement with our finding that $\bar{f}'^0_3$ is not linear with x in a conical 3D cell, Fig. 2.

To understand the generic scaling properties, we could once again integrate $\bar{f}'^p_n(x)$ numerically and fit it by a power law x^β. In general, in an n-ball, for $p > 1$, the exponent β appeared to increase with p independently of the dimension considered, but this result did not hold in an n-cone. As expected, for $p = 1$, we found $\bar{f}'^1_n(x)$ to be systematically linear with x, be the shape spherical or conical, Fig. 4. Interestingly, the 'cortical pulling' mechanism $\bar{f}'^0_n$ appeared linear only for a 3D spherical cell, and was not linear either for non-spherical cells or for $n \neq 3$. Thus, only the scaling $\bar{f}'^1_n(x) \propto x$ seems universal.

D. Effective stiffness

For both autonomous and directed centering, we next derived expressions for the effective stiffness in a spherical cell in n-dimensions. We defined the effective stiffness K^p_n, as :

$$K^p_n = -\partial_x \bar{f}^p_n\Big|_{x=0} \quad , \quad K'^p_n = -\partial_x \bar{f}'^p_n\Big|_{x=0} . \quad (17)$$

For *autonomous* centering, and in a spherical cell, we can keep the aforementioned definition of $l(\theta, x)$, see Eq. 2, and we find the stiffness (normalized by Nf_1/R) :

$$K^p_n = p\frac{\Gamma(n/2)}{\Gamma(1+n/2)} = \frac{p}{n}. \quad (18)$$

For *directed* centering, using Eqns. 11, 17, we can deduce the stiffness K'^p_n (normalized by Mf_m/R) in a sphere :

$$K'^p_n = \frac{n-1+p}{n} . \quad (19)$$

The dependence on n and p of the stiffness is very different from the *autonomous* centering case, compare Eq. 18, further highlighting the fundamental differences between autonomous and directed centering.

E. Definition of the cell center

As mentioned, in non-spherical cells, the aster seems to find the center of mass [1]. We therefore inquired which equilibrium position x^* may be reached in different centering mechanisms. Surprisingly, neither autonomous nor directed mechanism converged strictly to the center of mass of the space, Fig.4, bottom. Interestingly, x^* was not even necessarily monotonous in p (e.g. for $n = 3$). This highlights the non-trivial properties of centering forces. While this finding is theoretically interesting, it remains to be determined whether the predicted differences are within the range of experimental resolution in the case of pronucleus centering. More generally, this is to be kept in mind when using such centering schemes to find the center of a space.

F. Centering in non-convex spaces

Eventually, we studied centering mechanisms in a non-convex shape by considering a doublet of spheres, truncated on their Ox axis at $x = 0$, mimicking the geometry of a dividing cell, see Fig. 1. We took 3D spheres of radius $1/2 \leq r_1 \leq 1$, truncated at $x = 0$ and with centers at $x = -1 + r_1$ and $1 - r_1$, see Fig. 1. For such a shape, all the volume is not visible by any point in the sphere, and we do not expect $\bar{l}^n_n$ to be space invariant. Indeed, we found that the violation of the scaling law initially increases as r_1 decreases from 1, see Fig. 6, top. As the

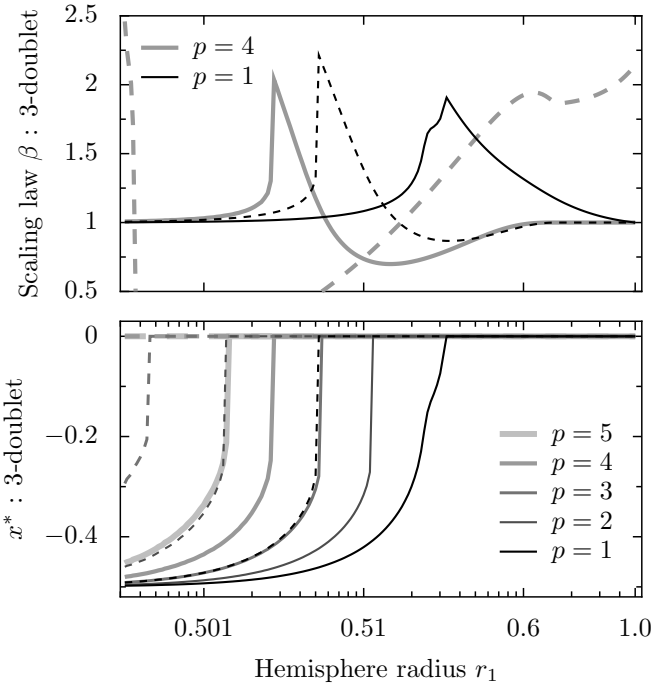

FIG. 6. *Top* : equilibrium position x^* such that $\bar{f}_3^p(x^*) = 0$ (autonomous centering, solid lines) and $\bar{f}'^p_3(x^*) = 0$ (directed centering, dashed lines) as a function of the hemisphere radius r_1 (log scale diverging at $r_1 = 0.5$). r_1 is defined such that $r_1 = 1$ for a single sphere and $r_1 = 0.5$ for a closed doublet. *Bottom* : Scaling law of $\bar{f}_3^p(x)$ (solid lines) and $\bar{f}'^p_3(x)$ (dashed lines) as a function of r_1.

doublet closes ($r_1 \to 1/2$), the scaling laws are restored because the visible space tends towards a single sphere.

We would also expect the center to be at $x^* = 0$ for $r_1 = 1$ (a spherical cell) and $x^* = \pm 0.5$ for $r_1 = 0.5$ (a perfect doublet). Indeed, we find a transition of x^* from 0 to 0.5 when $r_1 \to 1/2$. This transition happens after a threshold value of r_1 that depends on p ; whether this transition is continuous or not also depends on p, Fig. 6, bottom. This thus resembles a sub-critical pitchfork phase transition. Overall, the higher p, the higher the threshold value of r_1 both for autonomous and directed centering.

G. Alternative centering mechanisms

Beyond the biological context, another centering mechanism that could be considered is to minimize $\bar{l}_n^p(x)$. Going down the gradient of $\bar{l}_n^p$ yields a force $g_n^p(x) = -\partial_x \bar{l}_n^p(x)$. Note that an agent implementing such a strategy needs some kind of memory in order to compute the gradient, while the biologically relevant strategies require no memory. It is possible to show that :

$$g_n^p(x) = p\left(\frac{p-n}{p-1}\right)\bar{f}_n^{p-1}(x)\,. \tag{20}$$

Because of this result, the scaling properties of $g_n^p(x)$ are directly known from that of $\bar{f}_n^{p-1}(x)$. It is interesting to note that g_n^p is a centering force for $p > n$ and promotes decentering for $p < n$, and that, $\forall n$, $g_n^n(x) = 0$.

H. Discussion

We investigated the scaling properties of different centering mechanisms associated to microtubule forces: bulk pulling, pushing, and cortical pulling. In three dimensions, we found that bulk pulling exhibited surprising properties : the scaling of the force with the distance to the center was not straightforwardly given by the scaling of the individual microtubule forces. When the force per microtubule was proportional to microtubule length, the net centering force was proportional to the distance to the center, but only for a spherical cell. Similarly, cortical pulling had a force proportional to the distance to the center only in a spherical cell. However, we found that the linear scaling of $\bar{f}^4$ was independent of the geometry. Pushing can be mapped to the same problem as bulk pulling, but with a negative power law p. This analysis thus suggests that certain modes of microtubule force exertion may be more robust to cell shape or size variations, and could provide a theoretical rationale to understand evolutionary pressure that promote one mode of aster centering over another. It also matches previous findings that certain modes of centering can be more sensitive to asymmetric cues than other [5]. We did not consider dynamic processes such as aster oscillations and decentering. However, these processes are strongly controlled by the value of the centering stiffness (e.g. the amplitude of aster oscillations, or the extent of aster decentration) [2, 17, 18].

Experimentally, the stiffness K has been used to characterize the centering forces. In this letter, we clarified how K depends on dimensionality. This may be of broad biological relevance : rod-like cells like fission yeast have microtubules organized as a 1D array [19], and flat adherent cells might have an essentially 2D aster [20]. For 3D cells, 2D approximations of K can be off by up to 50%. More generally, K also depends on cell size in a way depending on p, which could be used experimentally to determine p if the centering mechanism is known. The stiffness only gives part of the story : to determine the centering mechanism, measuring the scaling of the force with x can be of high value. For example centering by pushing has a distinct scaling. While cortical and bulk pulling can yield the sale scaling for $\bar{f}(x)$ and $\bar{f}'(x)$, we showed that this scaling should depend differently on shape and size for these two modes of pulling. Therefore, measuring how K scales with R in one shape, and the scaling of the force with x in several shapes, should yield a unique choice of centering mechanism and of p [9, 10].

To reach more general understanding, we extended our study to an n-dimensional space. This allowed us to understand that the linear scaling of $\bar{f}_n^{n+1}(x)$ with x was

a general property in any convex space, while $\bar{f}_n^1$ was not necessarily linear with x. A generalization of cortical pulling showed no general reason for the linearity of $\bar{f'}_n^0(x)$ (which is indeed not universal), while $\bar{f'}_n^1(x)$ was always linear with x for a convex cell. At this stage, it is interesting to note that cortical pulling can be mapped to a generalization of Newton's shell, but not bulk pulling; those two mechanisms, with their different scaling properties, thus belong to different universality classes. Eventually, we also showed that the universal scaling laws break down when one assumption, the convexity of the space, is violated. For very non-convex cells, the 'centering' mechanisms may converge far from the geometric center. Biologically, this could be mitigated by other properties of the branching of microtubule networks, such as branching or nucleation away from the nucleus/centrosome. In such case we expect the exponent p to be some fractal dimension, or that equation 6 could be altogether broken. Even in convex cells, the definition of center is not necessarily straightforward. Neither centering mechanism actually led to the center of mass in a conical cell; rather, the zero-force position depends non-trivially on p and n.

These findings show a new behavior of a simple physical system. Further work on centering should include these non-trivial scaling properties. While this problem is inspired by biology, it has more generic applications, including the design of autonomous systems, or algorithms to find the center of a space.

I. Appendix : dynamic microtubules

We compute the fraction of microtubules touching the cortex at a distance l normalized by R. We take the most common assumption that microtubules may start depolymerizing (undergo *catastrophe*) with a rate c_0 upon touching the cortex ; if so, they depolymerize completely (no *rescue*). After a such event, microtubules start growing again at a speed v (normalized by R), and they can undergo no catastrophe until they touch the cortex. In this limit, the probability that a microtubule at a distance l from the cortex is pushing against it is $l_0/(l_0+l)$ with $l_0 = v/Rc_0$. In the regime $l_0 \gg 1$, most microtubules are pushing against the cortex and there little net centering. In the limit $l_0 \ll 1$, the probability for a microtubule to be pushing on the cortex is l_0/l, which should lead to centering.

III. ACKNOWLEDGEMENTS

The authors thank Hirokazu Tanimoto for the valuable suggestions, François Nédélec for suggestions on the manuscript, and Milan Lacassin for noticing the hypoelasticity of $\bar{f}_3^3$, thus inspiring this work. S.D. was supported by a CNRS-Momentum fellowship and N.M by an ERC consolidator grant (Forecaster 647073).

[1] Nicolas Minc, David Burgess, and Fred Chang. Influence of cell geometry on division-plane positioning. *Cell*, 144(3):414–426, 2011.

[2] Hirokazu Tanimoto, Jeremy Sallé, Louise Dodin, and Nicolas Minc. Physical forces determining the persistency and centring precision of microtubule asters. *Nature Physics*, 14(8):848–854, 2018.

[3] Stephan W Grill and Anthony A Hyman. Spindle positioning by cortical pulling forces. *Developmental cell*, 8(4):461–465, 2005.

[4] Martin Wühr, Sophie Dumont, Aaron C Groen, Daniel J Needleman, and Timothy J Mitchison. How does a millimeter-sized cell find its center? *Cell cycle*, 8(8):1115–1121, 2009.

[5] Gaëlle Letort, Francois Nédéléc, Laurent Blanchoin, and Manuel Thery. Centrosome centering and decentering by microtubule network rearrangement. *Molecular biology of the cell*, 27(18):2833–2843, 2016.

[6] Tamar Shinar, Miyeko Mana, Fabio Piano, and Michael J Shelley. A model of cytoplasmically driven microtubule-based motion in the single-celled caenorhabditis elegans embryo. *Proceedings of the National Academy of Sciences*, 108(26):10508–10513, 2011.

[7] Hai-Yin Wu, Ehssan Nazockdast, Michael J Shelley, and Daniel J Needleman. Forces positioning the mitotic spindle: theories, and now experiments. *Bioessays*, 39(2):1600212, 2017.

[8] Kenji Kimura and Akatsuki Kimura. A novel mechanism of microtubule length-dependent force to pull centrosomes toward the cell center. *Bioarchitecture*, 1(2):74–79, 2011.

[9] Anaëlle Pierre, Jérémy Sallé, Martin Wühr, and Nicolas Minc. Generic theoretical models to predict division patterns of cleaving embryos. *Developmental cell*, 39(6):667–682, 2016.

[10] Carlos Garzon-Coral, Horatiu A Fantana, and Jonathon Howard. A force-generating machinery maintains the spindle at the cell center during mitosis. *Science*, 352(6289):1124–1127, 2016.

[11] Jonathon Howard. Elastic and damping forces generated by confined arrays of dynamic microtubules. *Physical biology*, 3(1):54, 2006.

[12] Frederick Gittes, Brian Mickey, Jilda Nettleton, and Jonathon Howard. Flexural rigidity of microtubules and actin filaments measured from thermal fluctuations in shape. *The Journal of cell biology*, 120(4):923–934, 1993.

[13] Nenad Pavin, Liedewij Laan, Rui Ma, Marileen Dogterom, and Frank Jülicher. Positioning of microtubule organizing centers by cortical pushing and pulling forces. *New Journal of Physics*, 14(10):105025, 2012.

[14] Ruben Schmidt, Lars-Eric Fielmich, Ilya Grigoriev, Eugene A Katrukha, Anna Akhmanova, and Sander van den

Heuvel. Two populations of cytoplasmic dynein contribute to spindle positioning in c. elegans embryos. *J Cell Biol*, pages jcb–201607038, 2017.

[15] Ruddi Rodriguez-Garcia, Laurent Chesneau, Sylvain Pastezeur, Julien Roul, Marc Tramier, and Jacques Pecreaux. The polarity-induced force imbalance in caenorhabditis elegans embryos is caused by asymmetric binding rates of dynein to the cortex. *Molecular biology of the cell*, pages mbc–E17, 2018.

[16] Isaac Newton. The mathematical principles of natural philosophy.

[17] Stephan W Grill, Karsten Kruse, and Frank Jülicher. Theory of mitotic spindle oscillations. *Physical review letters*, 94(10):108104, 2005.

[18] Jérémy Sallé, Jing Xie, Dmitry Ershov, Milan Lacassin, Serge Dmitrieff, and Nicolas Minc. Asymmetric division through a reduction of microtubule centering forces. *J Cell Biol*, pages jcb–201807102, 2018.

[19] Guilhem Velve Casquillas, Chuanhai Fu, Mael Le Berre, Jeremy Cramer, Sebastien Meance, Adrien Plecis, Damien Baigl, Jean-Jacques Greffet, Yong Chen, Matthieu Piel, et al. Fast microfluidic temperature control for high resolution live cell imaging. *Lab on a chip*, 11(3):484–489, 2011.

[20] Jie Zhu, Anton Burakov, Vladimir Rodionov, and Alex Mogilner. Finding the cell center by a balance of dynein and myosin pulling and microtubule pushing: a computational study. *Molecular biology of the cell*, 21(24):4418–4427, 2010.